NJC

Accepted Manuscript

This article can be cited before page numbers have been issued, to do this please use: V. ANAND and D. Raghavachari, *New J. Chem.*, 2017, DOI: 10.1039/C7NJ01064H.

ROYAL SOCIETY OF CHEMISTRY

rsc.li/njc

View Article Online
DOI: 10.1039/C7NJ01064H

Journal Name

ARTICLE

White light emission from fluorene-EDOT and phenothiazine-hydroquinone based D-π-A conjugated systems in the solution, gel and film forms

Received 00th January 20xx,
Accepted 00th January 20xx

DOI: 10.1039/x0xx00000x

www.rsc.org/

Vivek Anand and Raghavachari Dhamodharan*

Two conjugated D-π-A organic molecules, one fluorene-ethylene dioxythiophene (**FL-E**) based and another phenothiazine-hydroquinone (**PT-Hq**) based were synthesized and observed to form 1-dimensional microstructures in solid state. These two molecules when mixed with rhodamine B dye (**Rh-B**) and photoexcited at 411 nm, generated white light with Commission Internationale d'Eclairage (CIE) coordinates (0.32, 0.33) in solution state. Similarly, white light was also obtained in the poly(methyl methacrylate) film (0.30, 0.33) and in gelatine gel (0.31, 0.34) for the same composition of the mixture as in the solution state. The correlated colour temperatures obtained in the three phases (6111 K in solution, 6900 K in PMMA film and 6400 K in gelatin gel) suggest that the system emits cool white light. In order to verify the D-π-A nature of the molecules, intramolecular charge transfer studies were done, which revealed that both the molecules showed positive solvatochromism. The plausible mechanism behind white light emission is Forster resonance energy transfer accompanied by simultaneous emission. This was verified through fluorescence titration experiment, lifetime studies, spectral overlap and Forster distance calculations and correlated to results from cyclic voltammetry and DFT studies. This is the first report on the emission of white light from D-π-A system by FRET.

Introduction

White light emitting devices, specifically white light emitting diodes (WLEDs) have gained enormous importance due to their potential applications in the fields of full colour panel displays, liquid crystal displays and back lighting sources.[1-5] Organic materials owing to their low cost, light weight, flexibility, ease of synthesis and the ability to form ultra-thin films are preferred over their inorganic counterparts in white light applications.[6,7] White light in organic materials can be achieved either by blending of different components (simultaneous emission of the three primary colours blue, green, and red) or from a single organic moiety, fluorescence of which, covers the entire visible region.[8-10] However, due to the constraint imposed by Kasha's rule, it is very difficult for a single organic material to emit white light. Hence, multi component organic white light emitting materials are in high demand.[11,12]

Donor-acceptor (D-A) conjugated organic molecules by virtue of their electronic functions, are of immense importance in optoelectronic fields such as organic light emitting diodes (OLEDs), field effect transistors (OFETs) and solar cells.[13-15] The solution processability and choice of molecular design give extra edge to their applicability. Hence, implication of such donor-acceptor type molecules in white light emission can be of great use.

Although organic conjugated molecules have been used for white light emission, not many D-A type molecules have been exploited for the same.[16-18] For instance, in 2013, Baumgartner *et. al.* reported white light generation based on donor-acceptor type dithienophosphole. In the same year, Wang *et. al.* reported two weakly interacting donor-acceptor dyads exhibiting white photoluminescence through controlled acid protonation.[18] In both the reports, white light was obtained using concentrated acids viz. camphorsulfonic acid and trifluoroacetic acid, which are highly corrosive. It is important that such harsh conditions are avoided in the generation of white light. 1D nano- and micro- materials are more promising building blocks for optoelectronic devices as compared to zero dimensional (0-D) materials and in this context D-A type molecules that form one-dimensional (1-D) microstructural morphology are sought after.[19-21] Even though, solution phase white light generation is more common, the development of white light in gel and film form are of more applicability in optoelectronic devices.[22,23]

Several approaches have been used in producing white light viz. single molecular excited state intramolecular proton

Department of Chemistry, Indian Institute of Technology Madras, Chennai-600036, India; Email: damo@iitm.ac.in

† Footnotes relating to the title and/or authors should appear here.
Electronic Supplementary Information (ESI) available: [details of any supplementary information available should be included here]. See DOI: 10.1039/x0xx00000x

View Article Online
DOI: 10.1039/C7NJ01064H

transfer (ESIPT),[24,25] solvent assisted self-assembly,[22,26,27] ESIPT coupled aggregation induced enhanced emission (AIEE)[28,29] and fluorescence resonance energy transfer (FRET).[30-33] FRET is a phenomenon in which a donor moiety in its excited electronic state transfers its energy to an acceptor moiety. Conditions necessary for FRET to take place are appreciable overlap between the fluorescence spectra of the donor and the absorption spectra of the acceptor. Furthermore, the distance between the donor and the acceptor should be small enough for energy transfer to take place.[33,34]

In the above context, the use of non-harsh conditions and white light generation in all the three forms (viz. solution, film and gel) acquire significance. In this work, two conjugated D-π-A organic molecules were designed and synthesised; one fluorene and ethylenedioxythioiphene (EDOT) based (**FL-E**) and another phenothiazine and hydroquinone based (**PT-Hq**). The synthesis of **PT-Hq** is new while we reported the synthesis of **FL-E** recently.[35] The reasons for choosing the specific fused aromatic ring systems are: fluorene is a good hole transporter, has excellent thermal and chemical inertness as well as good solubility and high fluorescence quantum yield.[36-38] EDOT, on the other hand, exhibits high molar absorption coefficient (ε) and due to the presence of heteroatoms efficiently donates electrons.[39-43] Phenothiazine was chosen because of its non-planar puckered structure and high fluorescence.[44,45] The motivation behind the synthesis is that when **FL-E**, a blue emitter ($\lambda_{max}^{em.}$ = 440 nm) is mixed with **PT-Hq**, which is a green emitter ($\lambda_{max}^{em.}$ = 517 nm) and an orange coloured rhodamine B dye ($\lambda_{max}^{em.}$ = 579 nm), white light generation can be expected. Interestingly, due to aggregation defect, green emission was observed for **FL-E** in solid state (the solid state fluorescence spectrum of **FL-E** is shown in Fig. S1). Infact, the dialkylfluorene are known to show green emission in the solid state due to keto or aggregation defects.[46-48] The details of the emission and its mechanism were thoroughly examined by fluorescence titration, spectral overlap studies, fluorescence lifetime studies, electrochemical studies and DFT calculations. In order to establish the D-π-A nature of the molecules, intramolecular charge transfer (ICT) studies were also done. Moreover, the emission of white light in poly(methyl methacrylate) [PMMA] film and gelatine gel forms are also obtained.

Results and discussion

Synthesis

The synthesis of **FL-E** was reported by us recently in another context.[35] For the synthesis of **PT-Hq** (for complete numbering of the molecules, please refer to Scheme S1), dialkynedioctyloxybenzene (**5**) was synthesised via Sonogashira reaction from 1,4-diiodooctyloxybenzene (**3**). The 1,4-diiodooctyloxybenzene (**3**) was synthesised by iodination of dioctyloxybenzene (**2**), which in turn was synthesized by the alkylation of hydroquinone (**1**). The bromoaldehyde (**9**) was obtained by the bromination of (**8**), which in turn, was obtained by the formylation of (**7**), preceded by alkylation of (**6**). Then, bromoaldehyde (**9**) was reacted with dialkynedioctyloxybenzene (**5**) to give **PT-Hq** via Sonogashira coupling reaction (Please see the detailed steps followed in the synthesis in Schemes S1**).** The structure of **PT-Hq** was characterized by the spectroscopic tools and found to be consistent with that expected (elaborate spectroscopic characterization and assignments are given in the supporting information Figs. S2-S7). The structures of blue, green and orange emitting fluorescent moieties viz. **FL-E**, **PT-Hq** and **Rh-B**, respectively, are shown in Scheme 1.

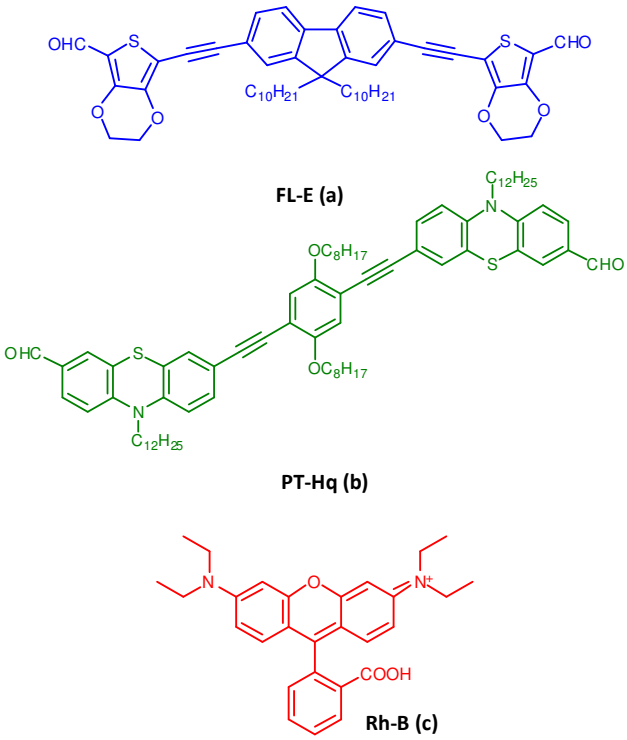

Scheme 1: (**a-c**) Chemical structures of **FL-E**, **PT-Hq** and **Rh-B**, respectively.

Morphology

In the solid state, **FL-E** and **PT-Hq** formed 1D microwires as shown in Figure 1(a) and 1(b), respectively. The diameter of the microfibers obtained in the case of **FL-E** is 300-350 nm, while that in the case of **PT-Hq** is 150-200 nm. Microfibrous alignment was also obtained in hexane, THF and DMF solution for **PT-Hq**. The attainment of microfibers in solution and solid phase depicts the strength of efficient π-π stacking, despite the presence of long alkyl chain, which is not very common in the case of organic molecules. This property could enable their use in nanolaser and other nano- and micro- optical devices.[49]

ICT studies

In order to confirm the D-π-A nature of the molecules **PT-Hq** and **FL-E**, intramolecular charge transfer studies were done.

View Article Online
DOI: 10.1039/C7NJ01064H

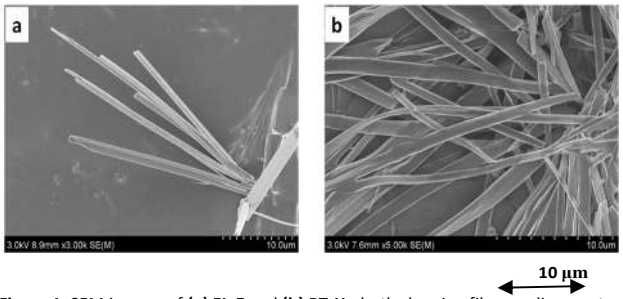

Figure 1. SEM images of **(a) FL-E** and **(b) PT-Hq** both showing fibrous alignment

The emission spectra of **PT-Hq** in nine different solvents with different polarities were recorded as shown in Figure 2(a). It was found that from hexane (λ_{max} = 492 nm) to THF (λ_{max} = 520 nm) there was a red shift of 28 nm in the emission λ_{max}. Furthermore, from THF to DMSO (λ_{max} = 543 nm) there was again a red shift of 23 nm in the λ_{max}. This red shift was accompanied by decrease in fluorescence intensity. These results suggest that the molecule shows positive solvatochromism.[50-52] Moreover, in order to get insight into the ICT nature, the emission energy versus solvent polarity study (Lippert-Mataga plot) was carried out as shown in Figure 2(b). A plot of the solvent polarity versus maximum emission energy (cm^{-1}) gave a straight line. The linear nature of the curve shows that only one excited state is present.[53,54] Similarly, in the case of **FL-E** a red shift of 35 nm was observed in the λ_{max} of the fluorescence spectrum as the polarity is changed from hexane to DMF. The spectrum is shown in Figure S8. Thus, both the molecules showed ICT properties, which confirm their D-π-A nature.

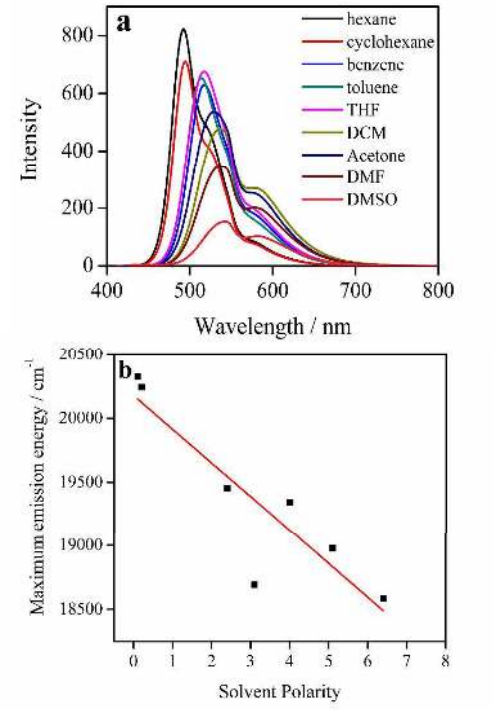

Figure 2. **(a)** ICT studies of **PT-Hq** in different solvents **(b)** Lippert-Mataga plot for **PT-Hq**

White Light Emission (in Solution, Film and Gel Phases)

The absorption spectra of **FL-E** (in THF), **PT-Hq** (in THF) and **Rh-B** (in water) showed absorption maxima at 406 nm, 411 nm and 553 nm, respectively. While the emission maxima for **FL-E**, **PT-Hq** and **Rh-B** are at 440 nm, 517 nm and 579 nm, respectively. The UV-visible and fluorescence spectra of each of the materials are shown in Figure 3. Inset shows the photographs of the corresponding materials in solution state under UV light.

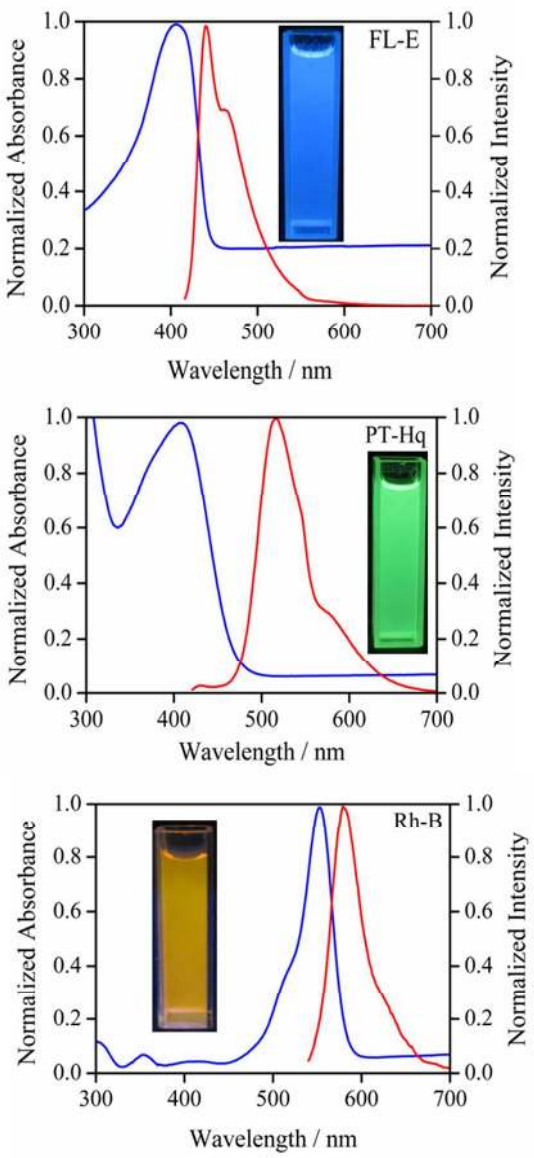

Figure 3. UV-Visible and fluorescence spectra of **FL-E**, **PT-Hq** and **Rh-B** ($\lambda_{exc.}^{em.} = \lambda_{max}^{abs.}$). Inset shows the photographs of their respective solutions under UV light irradiation

When 1 mL of **FL-E** (in THF) was mixed with 1 mL of **PT-Hq** (in THF) and 1.4 mL of **Rh-B** (in water), each of initial concentrations 10^{-5} M, and excited with UV light of wavelength 411 nm, the mixture exhibited two fluorescence bands at 477

View Article Online
DOI: 10.1039/C7NJ01064H

nm and 585 nm, respectively, as shown in Figure 4(a). It also emitted white light with a commission Internationale de L'eclairage (CIE) coordinates of x = 0.32, y = 0.33, which is almost equal to the standard CIE for white light viz. (0.33, 0.33) and correlated colour temperature (CCT) of 6111 K, as shown in Figure 4(b).

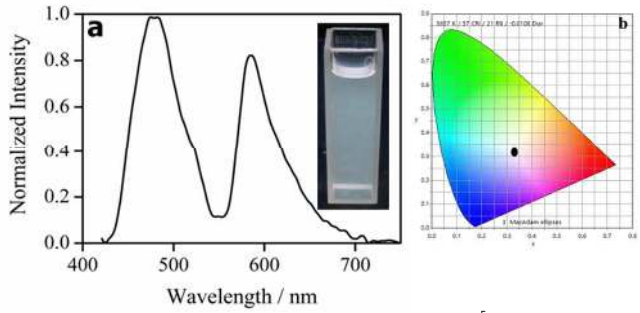

Figure 4. (a) Emission spectrum of mixture of **FL-E** (1 mL of 10^{-5} M, in THF), **PT-Hq** (1 mL of 10^{-5} M, in THF) and **Rh-B** (1 mL of 10^{-5} M, in water) in solution state, excited at 411 nm. Inset shows the photograph of corresponding white light under UV excitation. **(b)** CIE diagram of the corresponding white light emission in solution state.

The effect of change in the concentration of the molecules on white light emission was studied. At first, the concentration of **FL-E** and **PT-Hq** were kept constant at 1 mL (10^{-5} M each) and the concentration of **Rh-B** was increased in aliquots of 0.2 mL (10^{-5} M). At 1:1:1 ratio of **FL-E:PT-Hq:Rh-B**, the emission intensity due to the peak at 585 nm (mainly due to **Rh-B**) was not equivalent to the peak around 477 nm. The initial results suggest that the value of spectral overlap between **FL-E** and **PT-Hq** was 7.6×10^{14} M^{-1} cm^{-1} nm^4, which is higher than that for **PT-Hq** and **Rh-B** (4.88×10^{14} M^{-1} cm^{-1} nm^4). It was also evident from the quantum yield values that significant energy transfer was taking place from the blue to green component (Φ_{PL} = 0.48) as compared to the green to red component (Φ_{PL} = 0.18). Hence, the intensity mismatch was probably due to the lesser energy transfer from **PT-Hq** to **Rh-B** as compared to that from **FL-E** to **PT-Hq**. In order to achieve the pure white light emission (0.33, 0.33), the concentration of the red component was increased. At higher concentration, the emission intensity of the red component was increased as a result of partial energy transfer from **FL-E** followed by **PT-Hq**. Hence, 1:1:1.4 molar ratios was the optimized value to get pure white light. The CIE diagram with changing concentration of **Rh-B**, keeping **FL-E** and **PT-Hq** constant is shown in Fig. 5a, while the fluorescence spectra is shown in Fig. 5b. Similarly, the concentration of **PT-Hq** was varied, keeping the concentration of **Rh-B** and **FL-E** constant, the results of which are shown in supporting information Fig. S9. Then, the concentration of **FL-E** was varied, keeping **PT-Hq** and **Rh-B** constant, the results of which are shown in supporting information Fig. S10. These did not lead to appropriate CIE. Thus, the intensity match of the two peaks is critical for efficient white light emission. This intensity match depends on energy transfer and hence on spectral overlap between the molecules, which eventually leads to efficient white light emission.[34]

In control experiments, **FL-E** and **Rh-B** (1 mL each of initial concentration 10^{-5} M) were mixed. The emission spectrum corresponding to this mixture is shown in Fig. S11. The CIE coordinates for this emission (0.30, 0.29) does not correspond to pure white light (CIE diagram is shown in Fig. S12). Moreover, no white light was obtained in gel or film form by the combination of these two moieties in the same proportion as in solution. In another control experiment, **FL-E** and **PT-Hq** were mixed (1 mL each of initial concentration 10^{-5} M) and excited with UV light of wavelength 411 nm. The CIE obtained was (0.20, 0.28) and does not correspond to white light emission. The results from this study are shown in Fig. S13. Similarly, **PT-Hq** and **Rh-B** were mixed (1 mL each of initial concentration 10^{-5} M) and excited at the wavelength of 411 nm, to give a greenish-orange light with CIE coordinates (0.44, 0.52). This data is presented in Fig. S14. Thus, no efficient white light was obtained by the mixing of any two of these molecules. The mixing of all three components in the mole ratio 1:1:1.4 is a prerequisite for the attainment of efficient white light as confirmed by the test experiments.

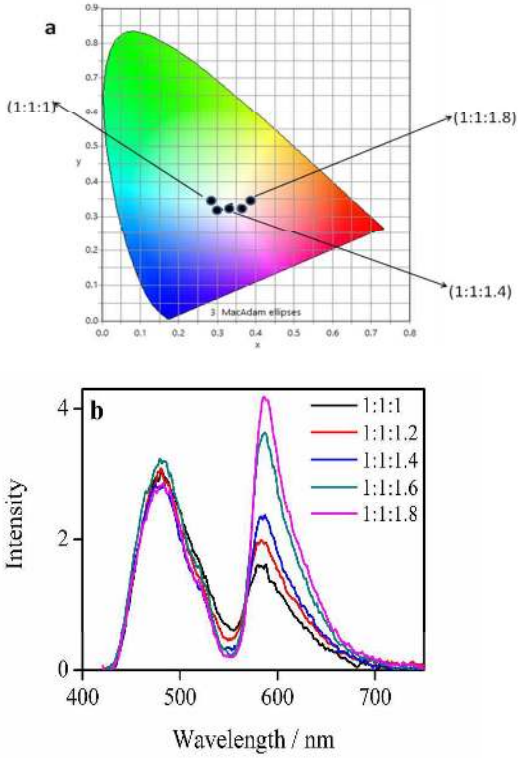

Figure 5. (a) CIE chromaticity diagram obtained on changing the volume of **Rh-B** from 1 mL to 1.8 mL, while keeping the volume of **FL-E** and **PT-Hq** at 1mL each. **(b)** The corresponding fluorescence titration spectra.

The emission of the mixture was studied in the film form (PMMA) and the result is shown in Fig. 6(a). The film showed two fluorescence bands at 494 nm and 590 nm. The CIE coordinate obtained is (0.30, 0.33) [the CIE diagram is shown in Fig. 7(a)] with a CCT of 6900 K. This means that the film emits cool white light. The white light emission was quite stable even after two weeks of the formation of film. Although the colour of the film was pale pink under the normal light, it showed white light when illuminated by UV light as shown in the inset of Fig. 6(a). In order to further broaden its utility, the

View Article Online
DOI: 10.1039/C7NJ01064H
Journal Name ARTICLE

emission of light was investigated in the gelatin gel phase. In this case, two fluorescence bands were observed at 471 nm and another at 581 nm, respectively, as shown in Fig. 6(b). The peak around 471 nm is quite broad and may be because of the combination of peaks due to the mixing of **FL-E** and **PT-Hq**. In gel, the CIE coordinates obtained was (0.31, 0.34) [CIE diagram is shown in Fig. 7(b)] and the CCT of 6400 K was obtained. Thus, white light was obtained with excellent CIE in all three phases viz. solution, PMMA film and gelatin gel. The emission was quite persistent and did not lose its white colour even after two weeks. The CCT obtained in all three cases hints towards cool white light emission. The attainment of white light in gel as well as film form enhances its applicability as solid state emitters are always preferred over their solution phase counterparts, from device fabrication point of view in optoelectronic applications.

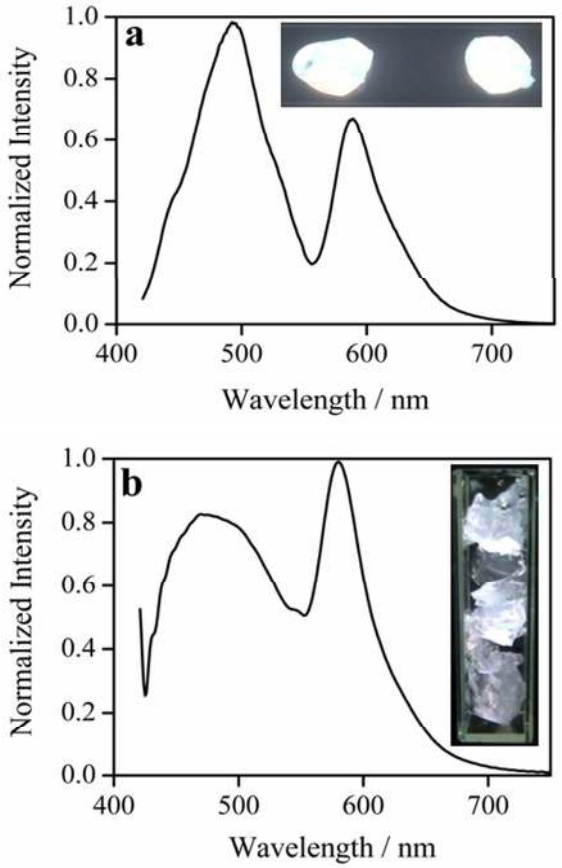

Figure 6. (a) Emission spectrum resulting from the mixture of **FL-E** (10^{-5} M, in THF), **PT-Hq** (10^{-5} M, in THF) and **Rh-B** (10^{-5} M, in water) in PMMA film, excited at 411 nm. Inset shows the photograph of corresponding white light under UV excitation. (b) Emission spectrum of mixture of **FL-E** (10^{-5} M, in THF), **PT-Hq** (10^{-5} M, in THF) and **Rh-B** (10^{-5} M, in water) in gelatine gel, excited at 411 nm. Inset shows the photograph of corresponding white light under UV excitation.

Deducing the Mechanism

Calculation of spectral overlap J(λ), rate of energy transfer *k* and distances r, R_o:

The rate of energy transfer was calculated using the formula:

$$k = \frac{E}{(1-E)\tau_D} \quad (1)$$

where,

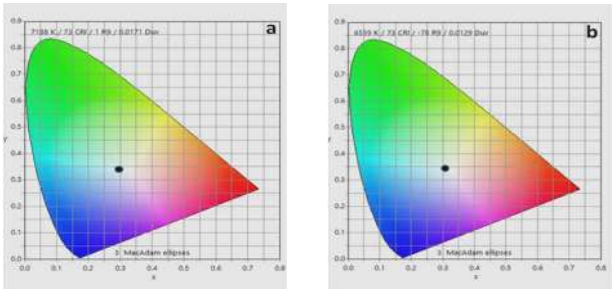

Figure 7. (a) CIE diagram of the corresponding white light emission in PMMA film. **(b)** CIE diagram of the corresponding white light emission in gelatin gel

E is the efficiency of energy transfer, τ_D is the lifetime of the donor in absence of acceptor. The distance between donor and acceptor was calculated by the formula:

$$r = \frac{R_o}{\sqrt[6]{k \times \tau_D}} \quad (2)$$

R_o is the Forster distance, the distance at which rate of energy transfer is 50 %. The Forster distance was calculated by the formula:

$$R_o = 0.211[\kappa^2 \times n^{-4} \times Q_D \times J(\lambda)]^{1/6} \quad (3)$$

where, κ^2 is the orientation factor (the value of κ^2 is taken as 2/3), n is the refractive index of the medium, Q_D is the quantum yield of the donor in the absence of acceptor and J(λ) is the spectral overlap.

The spectral overlap J(λ) was calculated using the formula:

$$J(\lambda) = \int_0^\infty F_D(\lambda)\varepsilon_A(\lambda)\lambda^4 d(\lambda) = \frac{\int_0^\infty F_D(\lambda)\varepsilon_A(\lambda)\lambda^4 d(\lambda)}{\int_0^\infty F_D(\lambda) d(\lambda)} \quad (4)$$

where, $F_D(\lambda)$ is the corrected fluorescence intensity of the donor in the wavelength range of λ to λ + Δλ with the total intensity (area under the curve) normalized to unity and ε_A is molar extinction coefficient of the acceptor.

The transfer energy was calculated using the formula:

$$E = 1 - \frac{\tau_{DA}}{\tau_D} \quad (5)$$

where, τ_{DA} is the lifetime of the donor along with the acceptor and τ_D is the lifetime of the pure donor.[55]

In order to investigate the mechanism of white light emission, the absorption and emission spectrum of the individual components were compared. This reveals that there is sufficient overlap between the emission spectrum of the donor to the absorption spectrum of the acceptor molecules as shown in Figure 8. The quantum yields for the emission of **FL-E** and **PT-Hq** were measured using fluorescein and anthracene, respectively, as standards in THF. The quantum yields for the emission are found to be 0.43 and 0.57 for **FL-E** and **PT-Hq,** respectively (the formula used to calculate quantum yield is given in eq. S1). The quantum yield for the emission of rhodamine B, as obtained from literature is 0.31 in water.[56]

To investigate the mechanism of white light emission further, the spectral overlap J(λ), Forster distance between the

View Article Online
DOI: 10.1039/C7NJ01064H

donor and acceptor were assessed. A significant overlap between the emission spectra of **FL-E** and the absorption spectra of **PT-Hq** was observed in the solution state as shown in Figure 8(a). In fact, the spectral overlap J(λ) for the system was found to be 7.6×10^{14} M^{-1} cm^{-1} nm^4 as calculated using eq. 4. The Forster distance between the donor **FL-E** and acceptor **PT-Hq**, as calculated from eq. 3 is 4.11 nm, which is within the expected range for smooth RET. A good spectral overlap between the emission spectrum of **PT-Hq** and the absorption spectrum of **Rh-B** was also observed as shown in Figure 8(b). The spectral overlap J(λ) was calculated using eq. 4 and was found to be 4.88×10^{14} M^{-1} cm^{-1} nm^4. The Forster distance was found to be 4.08 nm (eq. 3). The rate of energy transfer was also determined using eq. 5 and eq. 1, and was found to be 12.4×10^7 s^{-1}. Finally, the distance between the donor and the acceptor was calculated using eq. 2 and was found to be 4.5 nm. The emission spectrum of **FL-E** was also observed to overlap significantly with the absorption spectrum of **Rh-B** as shown in Figure 8(c). The spectral overlap integral J(λ) was calculated to be 2.94×10^{14} M^{-1} cm^{-1} nm^4, although the value is less than that for **FL-E** & **PT-Hq** and **PT-Hq** & **Rh-B** pairs. The essential conditions for FRET to take place are: appreciable overlap between the fluorescence spectra of the donor and the absorption spectra of the acceptor; and the distance between the donor-acceptor chromophore (Forster distance) should be between 1-10 nm. All the values obtained in this case agree with the above mentioned criterion and hence strongly correspond to the possibility of FRET.

Fluorescence Titration

The change in the fluorescence intensity of the donor molecule in the presence of the acceptor molecule (fluorescence titration) was studied to investigate the mechanism of emission further. To a solution of **FL-E** in THF (1 mL of 10^{-4} M), **PT-Hq** was added such that there was a gradual increase in the concentration of **PT-Hq** from 1 μM to 6 μM, keeping the concentration of **FL-E** constant (For example, at first 1 mL each of 10^{-4} M **FL-E** was taken in 7 cuvettes; then in the first cuvette 9 mL of THF was added to give a solution of 10^{-5} M solution of **FL-E**. In the second cuvette, 8 mL of THF was added along with 1 mL of 10^{-5} M **PT-Hq**, to give 10^{-5} M **FL-E** and 1 μM **PT-Hq.** Similarly, other solutions were made.). This resulted in a decrease in fluorescence intensity of the donor moiety with the concomitant increase in fluorescence intensity of the acceptor as shown in Fig. 9(a). For each 1 μM addition of **PT-Hq** solution, there was a decrease in fluorescence intensity at around 440 nm, while there was a gradual increase in fluorescence intensity at around 517 nm. There was also a gradual red shift in the emission peak due to **PT-Hq** from 509 nm to 517 nm. This observation suggests that energy transfer is taking place through FRET. Similar experiment was done starting from **PT-Hq** in THF to which **Rh-B** (in water) was added in lots 2 μM for each addition. Here again, there was a decrease in fluorescence intensity of donor moiety at around 517 nm, while there was a gradual increase in fluorescence intensity of the acceptor at around 590 nm as shown in Figure 9(b). There was also a gradual red shift in the emission peak of **Rh-B** from 584 to 590 nm. The initial sudden decrease in the intensities of **PT-Hq** may be due to the gradual addition of water, as water is a quencher of the fluorescence of **PT-Hq** as verified by ACQ experiments done for **PT-Hq**. The photoluminescence spectra of **PT-Hq** in THF/water mixture with 0 to 90 % water fraction is shown in Fig. S15. It can be seen that as the concentration of water was increased, there was a continuous decrease in fluorescence intensity. To further confirm the FRET mechanism, to a solution of **FL-E** in THF (1 ml of 10^{-4} M), **Rh-B** (in water) was added such that there was a gradual increase in the concentration of **Rh-B** while that of **FL-E** was constant (10^{-5} M). In this case also, a decrease in the intensity of blue component with the gradual increase in the intensity of red component was observed on addition of each 1 μM concentration of **Rh-B** as shown in Figure 9(c), along with the red shift in the λ_{max} of **Rh-B** from 587 nm to 592 nm. The signature of FRET is simultaneous increase in the fluorescence intensity of acceptor with the gradual decrease in the intensity of donor on addition of increasing concentration of acceptor to a fixed concentration of donor. This is clearly evident in all the three cases.

Lifetime studies

To further verify if FRET could be operational, the fluorescence lifetimes of **PT-Hq** and **PT-Hq** along with **Rh-B** in solution phase were recorded. The average lifetime of the mixture of **PT-Hq** and **Rh-B** was found to be 2.66 ns, while that for pure **PT-Hq** was 3.98 ns (as shown in Fig. 10). Clearly, there is a decrease in the lifetime of the mixture as compared to pure **PT-Hq**. All these observations lead to the conclusion that FRET is responsible for the energy transfer taking place from **FL-E** to **PT-Hq** to **Rh-B.** Interestingly, there was energy transfer taking place directly from **FL-E** to **Rh-B**. The FRET mechanism is illustrated elaborately in Scheme 2.

Electrochemical studies

The electrochemical behaviour of the molecules **FL-E** (in DCM), **PT-Hq** (in DCM) and **Rh-B** (in water) was investigated in solution state as shown in Figure 11. The CV of the molecules envisaged an oxidation process with E_{onset} oxidation at 1.13, 0.62 and 0.15 V for **FL-E**, **PT-Hq** and **Rh-B**, respectively. In the case of **PT-Hq,** the oxidation process was reversible unlike **FL-E** and **Rh-B**, where irreversible oxidation took place. The onset of oxidation peak can be attributed to the formation of radical cation in the molecules. The irreversible reduction peaks were obtained at -0.98, -1.23 and -0.92 V for **FL-E**, **PT-Hq** and **Rh-B**, respectively. The redox potential of Fc/Fc^+ (standard value 4.8 eV with respect to vacuum) was observed at 0.33 V in 0.2 M terabutylammoniumhexafluorophosphate/DCM solution. Based on this, the HOMO and LUMO energy levels of the molecules were estimated using the equation.[57]

View Article Online
DOI: 10.1039/C7NJ01064H

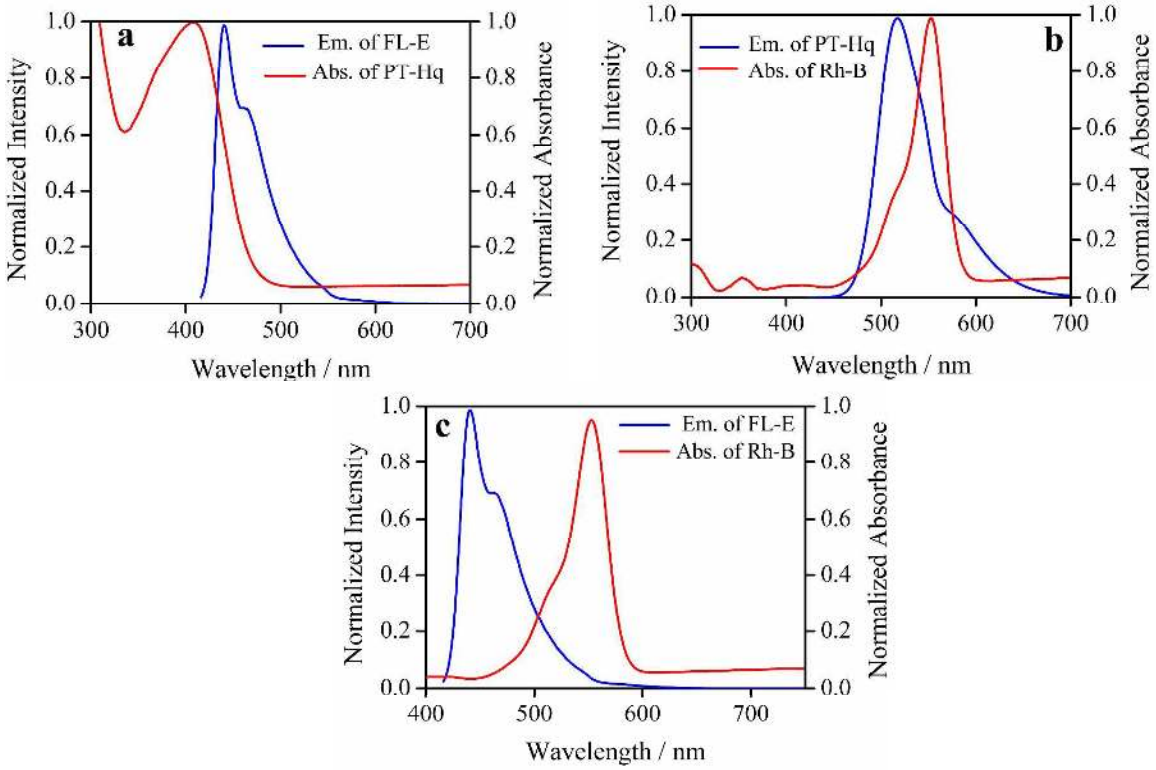

Figure 8. **(a)** Spectral overlap of fluorescence spectra of **FL-E** (blue) and absorption spectra of **PT-Hq** (red); **(b)** Spectral overlap of fluorescence spectra of **PT-Hq** (blue) and absorption spectra of **Rh-B** (red); **(c)** Spectral overlap of fluorescence spectra of **FL-E** (blue) and absorption spectra of **Rh-B** (red).

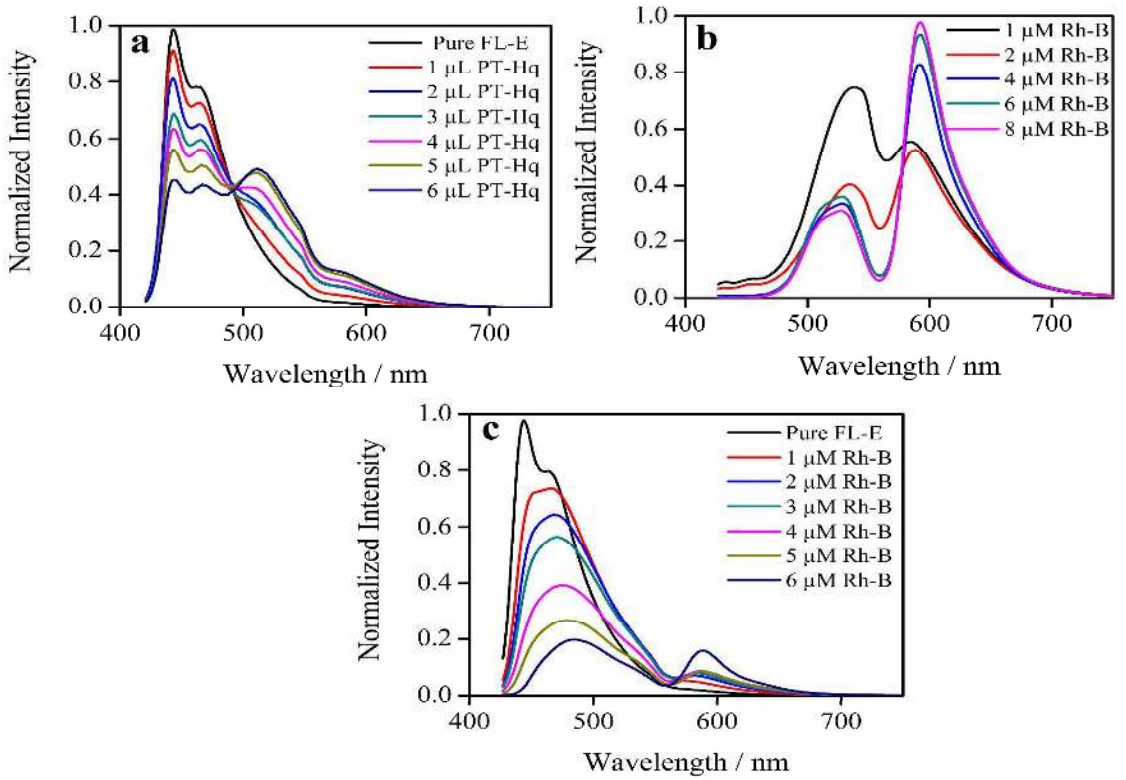

Figure 9. **(a)** Fluorescence spectra of **FL-E** (10^{-5} M, in THF) with the addition of **PT-Hq** (in THF) excited at 411 nm. **(b)** Fluorescence spectra of **PT-Hq** (10^{-5} M, in THF) with the addition of **Rh-B** (in water) excited at 411 nm. **(c)** Fluorescence spectra of **FL-E** (10^{-5} M, in THF) with the addition of **Rh-B** (in water) excited at 411 nm

View Article Online
DOI: 10.1039/C7NJ01064H

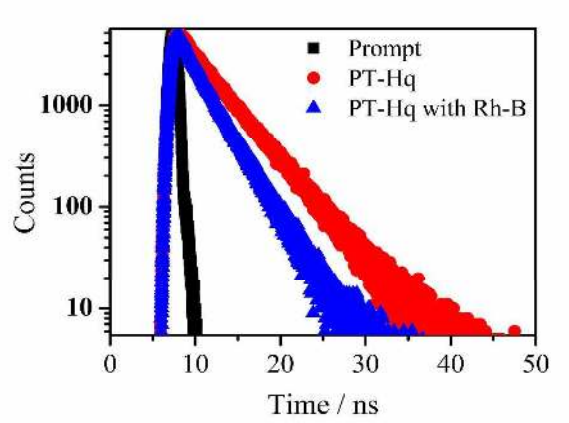

Figure 10. Fluorescence decay curves of pure **PT-Hq** (10^{-5} M in THF) and **PT-Hq** with **Rh-B** (10^{-5} M in water)

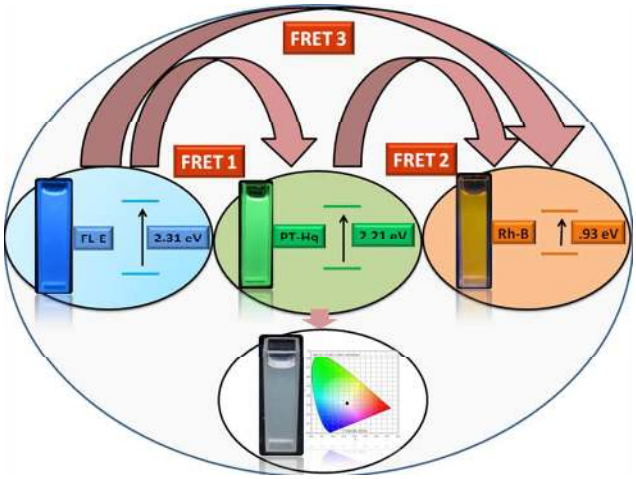

Scheme 2: Schematic presentation of FRET for the molecules **FL-E**, **PT-Hq** and **Rh-B** in solution along with their approximate energy level diagrams.

$$E_{HOMO} = - (E^{OX} + 4.47)\ eV \quad (6)$$

$$E_{LUMO} = - (E^{red} + 4.47)\ eV \quad (7)$$

where, E^{OX} and E^{red} are the onset potentials of oxidation and reduction, respectively, as measured against $Ag/AgNO_3$ reference for **FL-E** and **PT-Hq**, while Ag/AgCl electrode was used as reference for **Rh-B**. The HOMO energy levels of the molecules are -5.60, -5.09 and -4.62 eV for **FL-E**, **PT-Hq** and **Rh-B**, respectively. Thus, the HOMO levels decrease consecutively from blue (**FL-E**) to green (**PT-Hq**) to red (**Rh-B**), as expected. The LUMO levels, on the other hand, are -3.49, -3.24, -3.55 eV for **FL-E**, **PT-Hq** and **Rh-B**, respectively. The energy band gaps were calculated by subtracting the LUMO energy levels from HOMO energy levels. The electrochemical band gaps are found to be 2.11, 1.85, 1.07 eV for **FL-E**, **PT-Hq** and **Rh-B**, respectively. Furthermore, when the electrochemical band gaps were compared with those of optical band gaps, which were calculated from the solid state UV-visible spectra of the compounds, the values obtained were similar. The optical band gap was calculated using the formula $1240/\lambda_{onset}$. The values found are 2.14, 2.03 and 1.72 eV, respectively. The solid state UV-visible spectra of the compounds are shown in Fig. S16. Thus, energy band gaps decreases from **FL-E** to **PT-Hq** to **Rh-B**. This indicates that energy transfer may be possible between **FL-E** and **PT-Hq** and also between **PT-Hq** and **Rh-B**. Hence, electrochemical studies are also in agreement with the possibility of FRET and also enable better understanding of the positions of energy levels in the molecules.

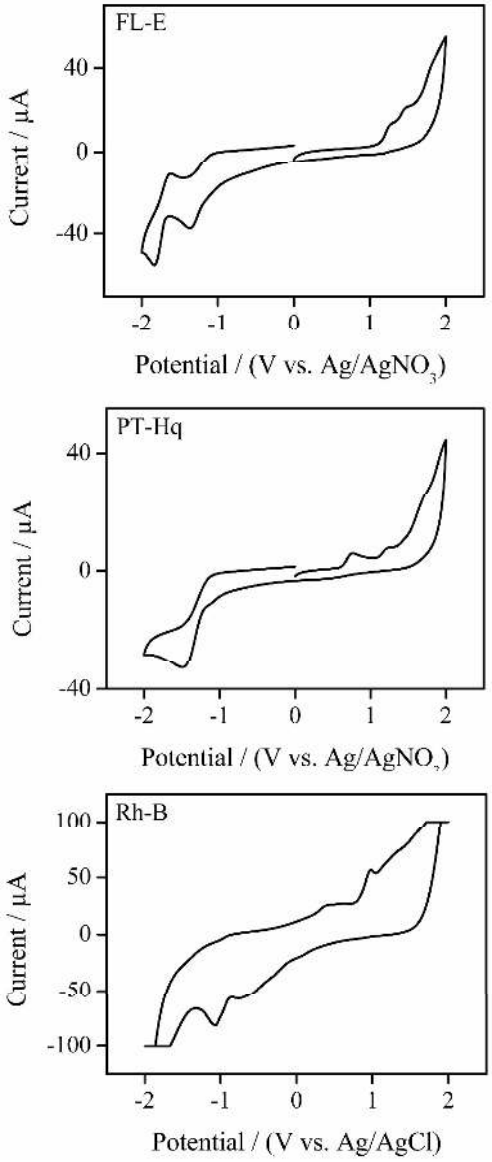

Figure 11. Cyclic voltammograms of **FL-E**, **PT-Hq** and **Rh-B** in solution state, 0.2 M Bu_4NPF_6 as supporting electrolyte for **FL-E** and **PT-Hq** while **0**.1 M KNO_3 as supporting electrolyte for **Rh-B.**

View Article Online
DOI: 10.1039/C7NJ01064H

DFT studies

Gas phase density functional theory (DFT) calculations (B3LYP/6-31G* level) were carried out to get insight into the electronic distribution and to study the chances of energy transfer between the molecules. The DFT generated HOMO and LUMO levels were also calculated for all the three molecules. The HOMO, LUMO pattern are shown in Figs. 12(a)-12(c).

In the case of **FL-E,** the HOMO is located on fluorene and on the sulphur atom of EDOT, while LUMO and LUMO + 1 degenerate orbitals are located on the oxygen atoms of EDOT (LUMO + 1 orbital is shown in Fig. S17). Oxygen being most electronegative carries most of the negative charge. Thus, the HOMO and LUMO levels are separated and localized. The HOMO energy level is 6.02 eV, while LUMO energy level is 3.71 eV and the energy band gap is 2.31 eV. This value is characteristic of blue emitters. On the other hand in **PT-Hq**, the HOMO-LUMO is uniformly delocalized throughout the molecule. This is common in case of molecules, which quickly deactivate after excitation and hence are highly emissive.[58] In fact, **PT-Hq** is highly emissive in the green region of the electromagnetic spectrum. Moreover, the theoretically calculated HOMO energy level is 5.11 eV, while LUMO energy level is 2.90 eV. This leads to energy band gap of 2.21 eV. In **Rh-B** the HOMO is located on the positively charged nitrogen atom, while LUMO is located throughout the molecule. The HOMO energy level is 4.10 eV and LUMO energy level is 3.18 eV, which gives energy band gap of 0.93 eV. Although, this value does not correspond to red emission, it is very close to it. Thus, the theoretically estimated values of energy levels and band gaps are similar to those of electrochemically determined values. When the theoretically calculated energy levels were compared, it was found that the values decrease gradually on moving from **FL-E** to **PT-Hq** to **Rh-B**. Hence this is an indication that energy transfer might be possible between the molecules. Thus, computational studies are also in agreement with the possibility of FRET. Furthermore, time dependent DFT studies (TDFT) were done to model the absorption process. The important electronic transitions along with the oscillator strength, wavelength and energy are shown in Table 1.

	Energy /cm^{-1}	λ /nm	Osc. Strength	Energy Levels
PT-Hq	21219	471.3	1.49	HOMO→LUMO (92 %)
FL-E	18908	528.8	0.30	HOMO→LUMO (84 %)

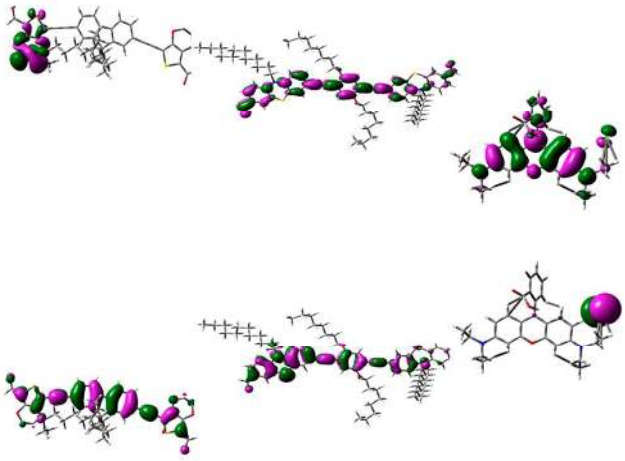

Figure 12. B3LYP/6-31G* DFT calculated HOMO (bottom) and LUMO (top) contours of **(a) FL-E (b) PT-Hq** and **(c) Rh-B**. The decrease in energy band gap from **(a)** to **(c)** is approximate (not drawn to the scale).

Conclusions

Two conjugated D-π-A organic molecules (**FL-E** and **PT-Hq**) were synthesized and observed to form 1D-microstructure in the solid state suggesting the presence of strong and efficient π-π interactions. These two molecules were mixed with rhodamine-B (**Rh-B)** dye in requisite proportion to produce white light in solution, PMMA film and gel phase. When mixed in molar ratio of **FL-E**:**PT-Hq**:**Rh-B** = 1:1:1.4, white light was obtained with CIE coordinates of 0.32 and 0.33 on excitation at 411 nm, the values being almost equal to that for pure white light. Similarly, the CIE obtained in film and gel form are (0.30, 0.33) and (0.31, 0.34), respectively. The combination of all three moieties (not any two) is crucial for white light emission as confirmed by the control experiments. Optimum correlated colour temperatures were also obtained in all the three cases. The values of CCT hint towards cool white light emission in all the three phases. The plausible mechanism for white light generation in solution state was found to be FRET as thoroughly studied by fluorescence titration, lifetime, and spectral overlap integral calculations. The energy band gaps as calculated from electrochemical studies were found to be 2.11, 1.85 and 1.07 eV for **FL-E**, **PT-Hq** and **Rh-B**, respectively. Thus, the decrease in band gaps from **FL-E** to **Rh-B** is an indicator of the probability of energy transfer. Furthermore, DFT studies agree with the possibility of FRET and were also used to study the electronic distribution and arrangements of the energy levels in all the three molecules. It was observed that the values of energy levels obtained from DFT studies are in agreement with those from electrochemical experiments.

View Article Online
DOI: 10.1039/C7NJ01064H

Experimental section

Materials.

Palladium (II) chloride [which was used to synthesise the catalyst $PdCl_2(PPh_3)_2$] and CuI were purchased from Sigma Aldrich and Finar & Co., respectively. The compounds 3,4-ethylenedioxythiophene and phenothiazine were purchased from Sigma Aldrich. Fluorene and hydroquinone were purchased from Alfa Aesar. All these chemicals were used as such without further purification. The solvents: DIPA, THF, DCM and toluene were purchased from Rankem & Co. and were distilled when necessary, using standard procedure. The deuterated solvents were purchased from Sigma Aldrich. Poly(methyl methacrylate) [PMMA] was purchased from L. G. Polymers while gelatin was purchased from S. D. fine-Chem. Pvt. Ltd.

Synthesis of PT-Hq

PT-Hq (new) was prepared using standard Sonogashira coupling reaction [Scheme 3]. The procedure is as follows: In a two-necked round bottom flask, the bromo-compound (**9**) (11.50 mmol, 2.2 eq.), Pd (II) (10 mol %), and CuI (10 mol %) were dissolved in a 1:1 mixture of solvents (DIPA:THF) (total 80 mL) and degassed for 15 minutes using argon. Then, a degassed solution of dialkyne (**5**) (5.23 mmol, 1 eq.) in THF was added through a syringe to the reaction mixture at room temperature (final solvent ratio = 1:1). Then, the temperature was raised to 70 °C and maintained for 12 h. After the reaction, the solvents were evaporated under vacuum and the residue was extracted with DCM and water, washed with brine solution, dried with Na_2SO_4 and filtered. The solvent was removed under vacuum and the resulting crude product was purified by silica gel column chromatography (hexane/DCM 3/2) to give the compound **PT-Hq**. Yield: 70 %, yellow solid. Mp. 89 °C. ^{1}H NMR (400 MHz, $CDCl_3$): δ 9.79 (s, 2H), 7.64 (d, *J* = 6.8 Hz, 2H), 7.57 (s, 2H), 7.31 (d, *J* = 6.8 Hz, 2H), 7.25 (s, 2H), 6.96 (s, 2H), 6.89 (d, *J* = 6.8 Hz, 2H), 6.81 (d, *J* = 6.8 Hz, 2H), 4.01 (t, *J* = 5.2 Hz, 4H), 3.88 (t, *J* = 6.0 Hz, 4H), 1.79-1.85 (m, 8H), 1.52-1.69 (m, 4H), 1.37-1.43 (m, 5H), 0.87-1.35 (m, 47H), 0.86-0.88 (m, 12H). ^{13}C NMR (125 MHz, $CDCl_3$): δ 190.0, 153.5, 150.0, 143.4, 131.3, 131.0, 128.5, 124.5, 123.8, 118.6, 116.7, 115.6, 115.0, 113.8, 93.9, 86.5, 69.6, 48.2, 32.0, 31.9, 29.7, 29.6, 29.5, 29.4, 29.3, 29.2, 26.8, 26.7, 26.2, 22.7, 14.2. IR (KBr): 2924, 2857, 1682, 1581, 1357, 1469, 1413, 1200, 820, 719, 552 cm^{-1}. UV-Vis (DCM) λ_{max}: 417 nm. MS (MALDI) *m/z*: 1168.72 (100 M^+). Anal. Calcd. for $C_{76}H_{100}N_2O_4S_2$: C, 78.04; H, 8.62; N, 2.39. Found: C, 78.35; H, 8.97; N, 2.50. All the spectral data with assignments are given in supporting information.

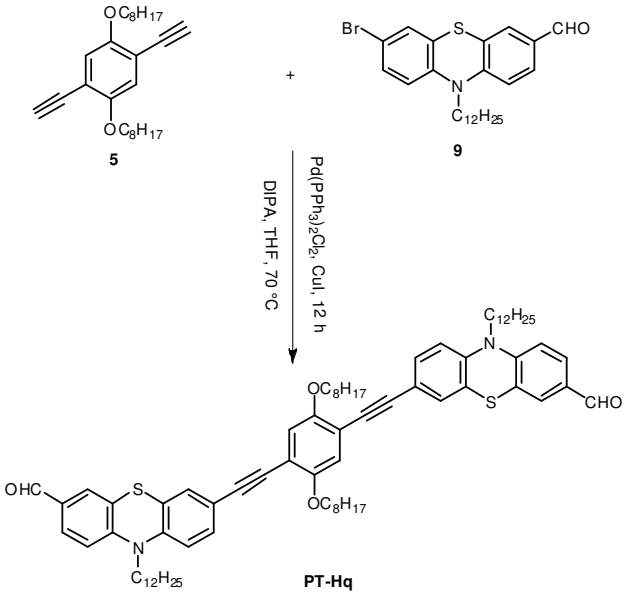

Scheme 3: Synthesis of **PT-Hq** (for complete numbering of the molecules please refer to **Scheme S1** of supporting information).

Polymeric film and gel preparation

Preparation of white light emitting PMMA film

PMMA film was prepared by adding 0.5 g of PMMA to a solution containing 1 mL of **FL-E** in THF, 1 mL of **PT-Hq** in THF and 1.4 mL of **Rh-B** in water, each of initial concentration 10^{-5} M. The viscous solution was kept overnight for drying at room temperature to obtain the desired film.

Preparation of white light emitting gelatin gel

Gelatin gel was prepared by dissolving 0.5 g of gelatine in 10 mL of distilled water (5 % w/v). To this viscous solution, the mixture of 1.4 mL of **FL-E** in THF, 1 mL of **PT-Hq** in THF and 1.4 mL of **Rh-B** in water (each of initial concentration 10^{-5} M) was added. The final mixture was heated to 65 °C, and then placed in the refrigerator, maintained at a temperature of 10 °C, overnight, to get the required white gel.

Characterization

Melting points were determined using SUNBIM (India) melting point apparatus. ^{1}H NMR spectra were measured on a BRUKER AVANCE 400 (400 MHz for ^{1}H) spectrometer. The chemical shift values of ^{1}H NMR are expressed in parts per million downfield relative to the internal standard, tetramethylsilane (δ = 0 ppm) or chloroform (δ = 7.26 ppm). Splitting patterns are indicated as s, singlet; d, doublet; t, triplet; q, quartet; m, multiplet. ^{13}C NMR spectra were measured on a BRUKER AVANCE 500 (125 MHz for ^{13}C) spectrometer with tetramethylsilane (δ = 0 ppm) or

View Article Online
DOI: 10.1039/C7NJ01064H

chloroform-d (δ = 77.0 ppm) as internal standard. Chemical shift values are given in parts per million downfield relative to the internal standard. UV-Visible absorption spectra were recorded on JASCO V-630 spectrophotometer. Fluorescence spectra and Quantum yield were measured on FLUOROMAX 4 (Horiba Jobin Yon). Infrared spectra (IR) were recorded on a JASCO FTIR–4500 spectrometer. Elemental analysis was carried out with PERKIN-ELMER CHN-2400 analyzer. The SEM images were recorded using an FEG Quanta 400 scanning electron microscope (electron acceleration voltage was 3 kV). Electrochemical analyses were carried out with a CHI 660D instrument using glassy carbon, silver electrodes (Ag/AgCl, Ag/$AgNO_3$) and platinum wire as working, reference and counter electrodes, respectively.

Acknowledgements

This work was supported by Indian Institute of Technology, Madras (IITM), India. Timely help from Suraj Kumar Panigrahi in lifetime studies is heartily acknowledged.

References

1 M. C. Gather, A. Kohnen and K. Meerholtz, *Adv. Mater*., 2011, **23**, 233-248.
2 M. Chen, Y. Zhao, L. Yan, S. Yang, Y. Zhu, I. Murtaza, G. He, H. Meng and W. Huang, *Angew. Chem. Int. Ed.,* 2016, **55**, 1-7.
3 S. Mukherjee, and P. Thilagar, *Dyes Pigm*., 2014, **110**, 2-27.
4 B. D`Andrade and S. R. Forrest, *Adv. Mater*., 2004, **16**, 1585-1595.
5 Y. Liu, M. Nishiura, Y. Wang and Z. Hou, *J. Am. Chem. Soc*., 2006, **128**, 5592-5593.
6 A. Kohnen, N. Riegel, J. H. W. M. Kremer, H. Lademann, D. C. Muller and K. Meerholz, *Adv. Mater*., 2009, **21**, 879-884.
7 T. Tsujimura, *OLED Display Fundamentals and Applications*, Wiley-VCH. 2012.
8 H. Wang, Q. Dong, J. Li, X. Fang, Y. Hao, H. Xu, B. Xu and W. Y. Wong, *J. Inorg. Organomet. Polym*., 2014, **24**, 201-207.
9 P. Malakar, D. Modak and E. Prasad, *Chem. Commun*., 2016, **52**, 4309-4312.
10 J. Liu, *Spectrochim. Acta Mol. Biomol. Spectrosc.,* 2015, **149**, 48-53.
11 B. Zhang, L. Liu and Z. Xie, *Isr. J. Chem*., 2013, **53**, 897-917.
12 M. Kasha, *Discuss. Faraday Soc.,* 1950, **9,** 14-19.
13 Z. H. Guo, Z. K. Jin, J. Y. Wang and J. Pie, *Chem. Commun*., 2014, **50**, 6088-6090.
14 P. Xue, B. Yao, J. Sun, Q. Xu, P. Chen, Z. Zhang and R. Lu, *J. Mater. Chem. C,* 2014, **2**, 3942-3950.
15 T. Jadhav, B. Dhokale, S. M. Mobin and R. Misra, *J. Mater. Chem. C,* 2015, **3**, 9981-9988.
16 X. H. Jin, C. Chen, C. X. Ren, L. X. Cai and J. Zhang, *Chem. Commun*., 2014, **50**, 15878-15881.
17 H. V. Huynh, X. He and T. Baumgartner, *Chem. Commun*., 2013, **49**, 4899-4901.
18 D. Liu, Z. Zhang, H. Zhang and Y. Wang, *Chem. Commun*., 2013, **49**, 10001-10003.
19 E. M. G. Frutos, *J. Mater. Chem. C,* 2013, **1**, 3633-3645.
20 L. Zhang, Y. Che and J. S. Moore, *Acc. Chem. Res*., 2008, **41**, 1596-1608.
21 X. Liu, D. Xu, R. Lu, B. Li, C. Qian, P. Xue, X. Zhang and H. Zhou, *Chem. Eur. J.,* 2011, **17**, 1660-1669.
22 P. Kumar, S. Soumya and E. Prasad, *ACS Appl. Mater. Interfaces,* 2016, **8***,* 8068-8075.
23 P. Pallavi, S. Bandyopadhyay, J. Louis, A. Deshmuk and A. Patra, *Chem. Commun*., 2017**, 53,** 1257-1260.
24 J. Zhao, S. Ji, Y. Chen, P. Guo and P. Yang, *Phys. Chem. Chem. Phys*., 2012, **14**, 8803-8817.
25 S. Achelle, J. R. Lopez, C. Katan and F. R. Guen, *J. Phys. Chem. C* 2016, **120**, 26986-26995.
26 R. Chakrabarty, P. S. Mukherjee and P. J. Stang, *Chem. Rev*., 2011, **111**, 6810-6918.
27 W. C. Geng, Y. C. Liu, Y. Y. Wang, Z. Xu, Z. Zheng, C. B. Yang and D. S. Guo, *Chem. Commun.,* 2017, **53**, 392-395.
28 Y. T. Lee, Y. T. Chang, C. T. Chen and C. T. Chen, *J. Mater. Chem. C,* 2016, **4**, 7020-7025.
29 S. Samanta, U. Manna and G. Das, *New J. Chem.,* 2017, **41**, 1064-1072.
30 P. Bairi, B. Roy, P. Chakraborty and A. K. Nandi, *ACS Appl. Mater. Interfaces,* 2013**, 5**, 5478-5485.
31 T. Pullerits and V. Sundstrom, *Acc. Chem. Res.,* 1996, **29**, 381-389.
32 K. V. Rao, K. K. Datta, M. Eswaramoorthy and S. J. George, *Chem. Eur. J*., 2012, **18**, 2184-2194.
33 V. Singh and A. K. Mishra, *Sci. Rep*., 2015, **5**, 11118.
34 D. K. Maiti, R. Bhattacharjee, A. Datta and A. Banerjee, *J. Phys. Chem. C,* 2013, **117**, 23178-23189.
35 V. Anand, E. Ramachandran and R. Dhamodharan, *J. Polym. Sci. Part A: Polym. Chem.* 2016, **54**, 2774-2784.
36 J. Lee, J. H. Cho, N. S. Cho, D. H. Hwang, J. M. Kang, E. Lim, J. I. Lee and H. K. Shim, *J. Polym. Sci. Part A: Polym. Chem*., 2006, **44**, 2943-2954.
37 B. B. Carbas, A. Kivrak and A. M. Onal, *Electrochim. Acta*., 2011, **58**, 223-230.
38 R. Wang, W. Z. Wang, G. Z. Yang, T. Liu, J. Yu and Y. Jiang, *J. Polym. Sci. Part A: Polym. Chem*., 2008, **46**, 790-802.
39 K. Lin, S. Zhen, S. Ming, J. Xu and B. Lu, *New J. Chem*., 2015, **39**, 2096-2105.
40 Y. Karzazi, *J. Mater. Environ. Sci*., 2014, **5**, 1-12.
41 N. A. Rice and A. Adronov, *Macromolecules,* 2013, **46**, 3850-3860.
42 A. Elscher, S. Kirchmeyer, W. Ovenich, U. Merker and K. Reuter, *PEDOT: Principle and Applications of an Intrinsically Conductive Polymer,* CRC Press*,* Taylor and Francis Group, 2010.
43 K. Takagi, E. Kawagita and R. Kouchi, *J. Polym. Sci. Part A: Polym. Chem*., 2014, **52**, 2166-2174.
44 L. Yang, J. K. Feng and A. M. Ren, *J. Org. Chem.,* 2005, **70**, 5987-5996.
45 G. Zhang, J. Sun, P. Xue, Z. Zhang, P. Gong, J. Peng and R. Lu, *J. Mater. Chem. C,* 2015, **3**, 2925-2932.
46 A. C. Grimsdale, *Curr. Org. Chem.*, 2010, **14**, 2196-2217.
47 K. L. Chan, M. Sims, S. I. Pascu, M. Ariu, A. B. Holmes and D. D. C. Bradley, *Adv. Funct. Mater*. 2009, **19**, 2147-2154.
48 C. Poriel, N. Cocherel, J. R. Berthelot, L. Vignau and O. Jeannin, *Chem. Eur. J.*, 2011, **17**, 12631-12645.
49 Y. Li, T. Liu, H. Liu, M. Z. Tian and Y. Li, *Acc. Chem. Res*., 2014, **47**, 1186-1198.
50 G. J. Zhao, R. K. Chen, M. J. Sun, J. Y. Liu, G. Y. Li, Y. L. Gao, K. L. Han, X. C. Yang and L. Sun, *Chem. Eur. J.* 2008, **14,** 6935-6947.
51 J. Zhang, B. Xu, J. Chen, L. Wang and W. Tian, *J. Phys. Chem. C* 2013, **117**, 23117-23125.
52 F. B. Dias, S. Pollock, G. Hedley, L. O. Palsson, A. Monkman, I. I. Perepichka, I. F. Perepichka, M. Tavasli and M. R. Bryce, *J. Phys. Chem. C* 2006, **110**, 19329-19339.

View Article Online
DOI: 10.1039/C7NJ01064H

53 C. Jia, S. X. Liu, C. Tanner, C. Leiggener, A. Neels, L. Sanguinet, E. Levillin, S. Leutwyler, A. Hauser and S. Decurtins, *Chem. Eur. J.* 2007,**13**, 3804-3812.
54 R. Hu, E. Lager, A. A. Aguilar, J. Liu, J. W. Y. Lam, H. H. Y. Sung, J. D. Williams, Y. Zhong, K. S. Wong, E. P. Cabrera and B. Z. Tang, *J. Phys. Chem. C* 2009, **113**, 15845-15853.
55 J. R. Lakowicz, *Principles of fluorescence spectroscopy*, 3rd ed., Springer: New York, 2006.
56 M. J. Snare, F. E. Treloar, K. P. Ghiggino and P. J. Thistlethwaite, *J. Photochem*., 1982, **18**, 335-346.
57 Y. Zhou, P. Peng, L. Han, W. Tian, *Synth. Met.* 2007, **157**, 502-507.
58 Y. Wang, X. Cheng, X. Yang and X. Yang, *J. Solution Chem*. 2006, **35**, 869-878.

View Article Online
DOI: 10.1039/C7NJ01064H

Journal Name

ARTICLE

Graphical Abstract

The appropriate composition of two new D-π-A conjugated organic molecules in combination with rhodamine B is observed to emit cool white light in solution and solid states.